Earth and Planetary Science Letters 452 (2016) 197–205

Contents lists available at ScienceDirect

Earth and Planetary Science Letters

www.elsevier.com/locate/epsl

Hydration state of calcium sulfates in Gale crater, Mars: Identification of bassanite veins

W. Rapin [a,b,*], P.-Y. Meslin [a,b], S. Maurice [a,b], D. Vaniman [c], M. Nachon [d], N. Mangold [d], S. Schröder [b], O. Gasnault [a,b], O. Forni [a,b], R.C. Wiens [e], G.M. Martínez [f], A. Cousin [a,b], V. Sautter [g], J. Lasue [a,b], E.B. Rampe [h], D. Archer [i]

[a] Université de Toulouse, UPS-OMP, Toulouse, France
[b] Institut de Recherche en Astrophysique et Planétologie, CNRS, UMR 5277, Toulouse, France
[c] Planetary Science Institute, Tucson, AZ, USA
[d] Laboratoire de Planétologie et Géodynamique de Nantes, CNRS, UMR6112, Université de Nantes, Nantes, France
[e] Los Alamos National Laboratory, Los Alamos, NM, USA
[f] University of Michigan, Ann Arbor, USA
[g] Muséum National d'Histoire Naturelle, Laboratoire de Minéralogie et Cosmochimie du Muséum, Paris, France
[h] Aerodyne Industries at NASA Johnson Space Center, Houston, TX, USA
[i] NASA Johnson Space Center, Houston, TX, USA

ARTICLE INFO

Article history:
Received 27 October 2015
Received in revised form 13 July 2016
Accepted 25 July 2016
Available online 17 August 2016
Editor: C. Sotin

Keywords:
Mars
calcium sulfate
bassanite
LIBS
hydrogen
ChemCam

ABSTRACT

In-situ analyses reveal the presence of hydrogen within calcium sulfate veins crosscutting the sediments found in Gale crater. Laboratory experiments were performed to calibrate the hydrogen signal measured by laser induced breakdown spectroscopy (LIBS) in a range applicable to martian data. The analyses indicate that all veins targeted so far at Gale consist predominantly of bassanite which most likely formed by dehydration of gypsum. This scenario suggests that the percolating water produced gypsum, possibly by hydration of anhydrite in aqueous solution, and remained at temperatures below ~60 °C at that time. Desiccating conditions followed, consistent with a hyperarid climate and favored by burial or impacts. Additionally, anhydrite with lesser bassanite has been found by XRD in samples of sediments hosting the veins. Our result suggests bassanite is likely found in the veins and anhydrite may be more common as a fine-grained component within the sediments.

1. Introduction

Calcium sulfates are relatively common evaporitic minerals which are found to hold structural water in three different phases: gypsum ($CaSO_4 \times 2H_2O$) with 20.9 wt.% water, bassanite ($CaSO_4 \times 0.5H_2O$) 6.2 wt.% (but variable), and anhydrite (anhydrous $CaSO_4$). Because these sulfates mostly form in the presence of water, they can hold information about past aqueous activity on Mars in terms of temperature, humidity and salinity.

Calcium sulfates have been identified on Mars from orbit in different states of hydration. In near-infrared reflectance spectroscopy, gypsum presents strong but similar spectral features to bassanite making the distinction difficult (Bishop et al., 2014). The anhydrous form is even more difficult to detect because it lacks diagnostic water absorption bands. Using data from orbital instruments, in particular Compact Reconnaissance Imaging Spectrometer for Mars (CRISM) and Observatoire pour la Minéralogie, l'Eau, les Glaces et l'Activité (OMEGA), gypsum dunes were identified in Olympia Planitia in the north polar region (Langevin et al., 2005) and light toned deposits with spectral signatures consistent with gypsum were also found at lower latitudes (Gendrin et al., 2005) in Iani Chaos (Gilmore and Greenwood, 2009) and Noctis Labyrinthus (Weitz et al., 2013). However, a horizontal unit in Mawrth Vallis presents signatures more consistent with bassanite (Wray et al., 2010) and a thin alteration layer described in Mangold et al. (2010) also has spectral features most similar to bassanite. CaO vs. SO_3 correlations were seen by the Alpha Particle X-Ray Spectrometer in Endurance crater on the Homestake white vein (Squyres, 2012). The APXS is not sensitive to hydrogen but PanCam filter

* Corresponding author at: IRAP/CNRS 9, avenue colonel Roche, 31028, Toulouse, France.
E-mail address: william.rapin@irap.omp.eu (W. Rapin).

http://dx.doi.org/10.1016/j.epsl.2016.07.045
0012-821X/

images suggested a hydration band near ~950 nm in the spectra acquired on the vein (Squyres, 2012). In most places where gypsum or bassanite deposits were identified in-situ or from the orbit, the spectral signatures were not strong enough to distinguish unambiguously the two hydrated species.

More recently, numerous calcium-sulfate veins were found in-situ at Gale crater using the ChemCam instrument (Nachon et al., 2014) onboard Curiosity. The veins cross-cut the stratigraphic column from the oldest to the most recent units, including various types of sediments (e.g., mudstones and sandstones). This fracture filling suggests that the aqueous activity occurred after sedimentation. Some vein material in the mudstone named John Klein was sampled by the rover drill in the Yellowknife Bay area and analyzed by the XRD instrument; no gypsum was found in the drill powders but small amounts of anhydrite and bassanite (respectively ~1 and 0.7 wt.%) were present (Vaniman et al., 2014). The rover mast color cameras (MastCams) have a series of spectral filters which cover the band depth at 900–1000 μm (Rice et al., 2013). Most of these multispectral images show no evidence for gypsum either, except a possible detection in some of the thick veins or nodules in the Yellowknife Bay area (Vaniman et al., 2014).

Given the ChemCam instrument's ability to detect hydrogen (Schröder et al., 2015), this study focuses on a calibration method to constrain the water content of the calcium sulfate veins targeted on Mars. We first present the experimental method and the signal processing used, then the calibrated result for the vein dataset at Gale crater. Finally the implications of the findings on the environment at the time of formation and during subsequent evolution are discussed based on the stability of the different calcium sulfate phases and kinetics of their formation and alteration.

2. Materials and methods

2.1. Instrument description

The ChemCam instrument provides elemental compositions of targets at remote distances using Laser Induced Breakdown Spectroscopy (LIBS) (Maurice et al., 2012; Wiens et al., 2012) as well as high resolution images with a Remote Micro Imager (RMI) (Le Mouélic et al., 2015). A pulsed laser (14 mJ, 5 ns) is focused through an optical system to create a plasma on targets located up to 7 m from the rover. The plasma, containing excited atoms and ions, is observed through the same optics but directed to a spectrometer to resolve the emission peaks. The hydrogen atom emits photons at the Balmer alpha wavelength of 656.6 nm. The spectrometer FWHM resolution at this wavelength is 0.65 nm. Other hydrogen peaks lie outside of the spectrometer detection range (240–342 nm, 382–469 nm, 474–906 nm).

For each laser shot, the target's ablated area is about 300 to 600 μm in diameter and a few micrometers in depth, depending on the targeted material. Due to the plasma-induced shockwave, dust is effectively removed by the first shots, enabling measurements of the substrate without influence from surface-deposited materials. This dust-removal ability is particularly important for studying the hydrogen content of rocks because a strong signal is reported in the martian dust both in situ (Meslin et al., 2013) and from orbital measurements (Audouard et al., 2014). Usual ChemCam observations consist typically of bursts of 30 laser shots on a given point; several points are generally analyzed at closely spaced locations on the target.

The ChemCam engineering qualification model, similar to the flight model (Maurice et al., 2012; Wiens et al., 2012) was used in this study to acquire LIBS spectra in the laboratory under conditions similar to Mars. The laser unit was maintained at a controlled temperature of −10 °C in a climate chamber and pointed towards a window similar to the one mounted on the remote warm electronics box designed for the flight instrument onboard Curiosity. The laser beam was directed toward the samples through a window into a Mars-pressure chamber, with the beam directed vertically downward by an adjustable mirror. The total pressure was set to ~7 mbar of CO_2 (with a few % of N_2 and argon similar to the martian atmosphere composition) and degassing did not increase by more than 0.05 mbar during the tests, which means that the relative humidity remained below 0.3%. A series of regularly-spaced LIBS points were observed on the target, similar to those performed on Mars with the ChemCam flight model. The spectra collected for each laboratory sample resulted from series of 30 laser shots on 8 locations. The instrument-to-target distance of 1.5 m results in a similar laser irradiance as obtained on Mars at distances between 2.5 and 3.5 m, where most of the Mars targets are located. Nonetheless, because of different end-to-end setups, the laser irradiance on target can differ from observations performed on Mars, so we used a data normalization method which has proved to correct this effect on the H signal (see Section 2.3 and Supplementary Material).

2.2. Sample preparation

Powders of pure gypsum and bassanite were pressed under 3 t into 1 cm-∅ pellets. Commercial chemical reagent powders were used, and mineral purity was verified independently using Raman spectroscopy. Anhydrite pellets were obtained from dehydration of bassanite pellets. Since the LIBS signal is known to depend on the chemical matrix of the sample, additional pellets made of mixtures of gypsum and basalt with varying gypsum content were used to assess this effect on the H calibration. The basalt, from Skjaldbreiður, Iceland (2709SKA), was crushed and sieved to a grain size finer than 63 μm then mixed with fine gypsum powder. To minimize the contribution of adsorbed water for bassanite, gypsum, and mixtures of gypsum and basalt, the samples were exposed to vacuum for 24 h at room temperature (~22 °C). In the case of anhydrite pellets, the samples were heated within the chamber at 750 °C under vacuum for 16 h. After the LIBS spectra were collected, the pellets' bulk water content was estimated using thermogravimetric analysis (TGA) with a moisture analyzer that heated the sample to 200 °C. Total water loss was reached within 1 h. The water content measured for the gypsum pellet matched the 20.1 wt.% stoichiometric value, and for the bassanite pellet it is near 6.2 wt.%, typical for the hemihydrate. The water content observed for mixtures of gypsum and basalt also matched the mixture stoichiometry.

2.3. Hydrogen data processing and normalization

Processing of the hydrogen LIBS signal was designed to extract the area of the hydrogen emission peak. Next to the hydrogen signal at 656.6 nm are carbon emission peaks grouped around 658 nm, forming a single peak in ChemCam spectra. During plasma expansion into the atmosphere, the breakdown of the atmospheric CO_2 produces this peak seen in every martian spectrum. Nearby iron peaks are also detected and clearly seen in the case of high iron targets (Fe I 654.8 nm and Fe I 659.4 nm). Because of their spectral proximity, the C and Fe peaks are fitted simultaneously in order to extract the proper H peak from the spectral region. We use a multi-Lorentz fitting method with a linear baseline similar to Schröder et al. (2015). Fig. 1 shows an example of the fit result for a high iron target, where the resulting fitted hydrogen Lorentz peak is shown in blue. The H peak area is then easily computed from the parameters of this peak. Moreover, for each LIBS point location, a spectrum without laser pulses is acquired in order to remove the background light from the target in the active spectra. As

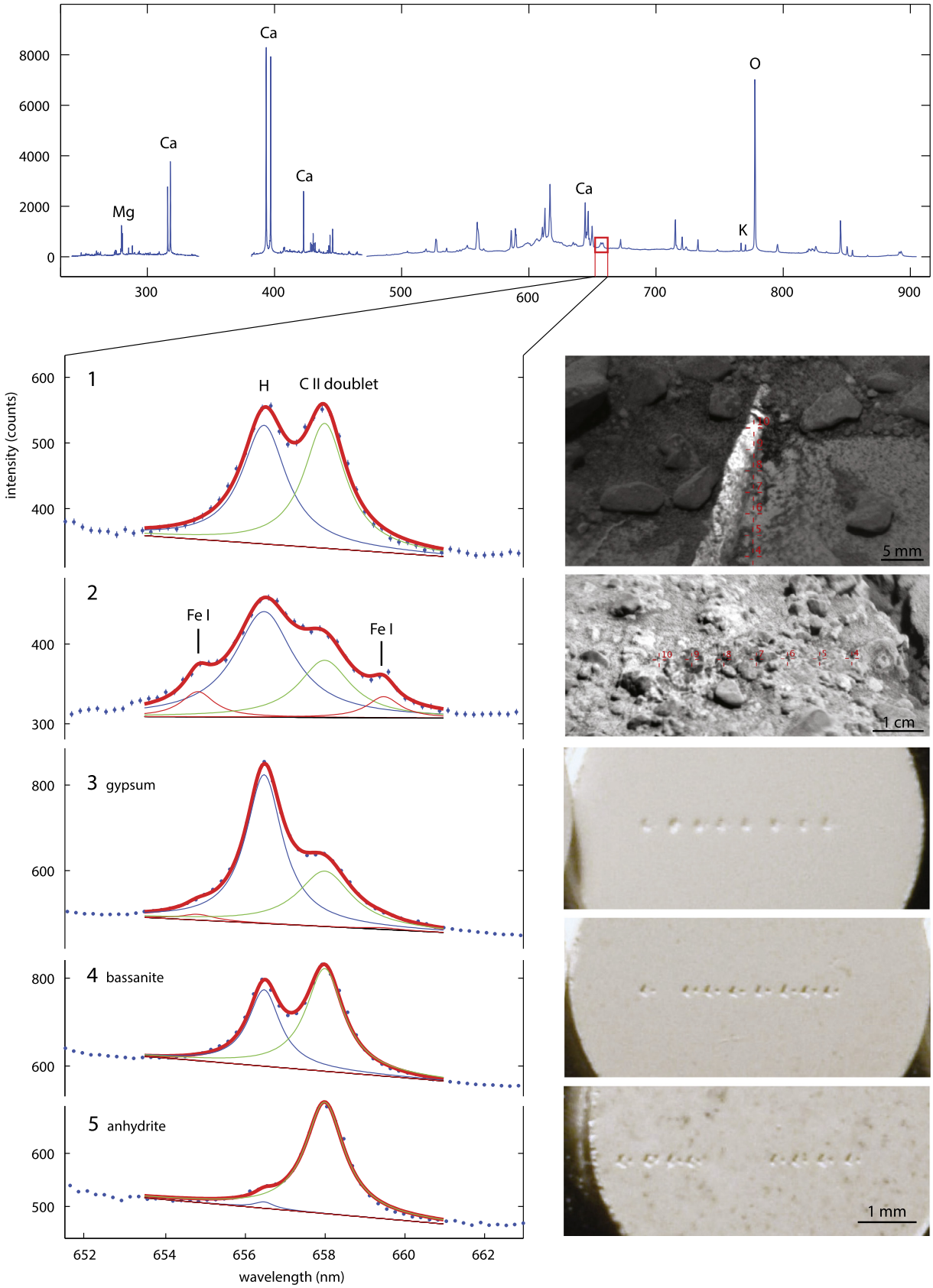

Fig. 1. Average total spectrum from the target "Bird Spring" point # 10 (top). Zoomed-in region shows the total emission profile (blue dots), with Lorentz peaks of hydrogen (blue), carbon (green) and the resulting fit (bold red) (1). Context RMI images for each sample are shown on the right, with annotated LIBS points. Example of a high-iron target (2) illustrates the presence of two iron peaks on the edges of the hydrogen and carbon peaks; the target shown here is "Butchers Gulley" with iron peak fits (red). The same LIBS spectral region is shown for laboratory pellets: gypsum (3), bassanite (4), anhydrite (5), and corresponding documentation images showing laser ablation pits on the surfaces of the pellets. Note the change of vertical scale between bassanite, gypsum and anhydrite.

shown by Schröder et al. (2015), this "dark removal" is particularly important to study the hydrogen signal because of the presence of the solar Balmer H absorption line observed in the background spectrum of targets illuminated by sunlight.

The LIBS hydrogen signal is known to vary because of many factors related to the technique. To correct for these effects, a normalization method must be applied to the signal. For the purpose of this study, an extensive set of factors affecting the hydrogen signal was investigated. Indeed, the H signal varies for instance with distance, laser energy, focus, crater depth, and the sample's physical and chemical matrix. Most of the available normalization methods have been tested, both in the lab and on Mars for most factors, i.e. normalization to the continuum spectrum, to the total peak intensity, to the oxygen peak (O I 778 nm unresolved triplet) and to the carbon peaks (C II 658 nm and C I 248 nm). As detailed in the Supplementary Material, comparisons between these methods showed that the normalization to the carbon peak at 247.9 nm efficiently corrects for most of the effects in a range enabling the use of a majority of the Martian data. The other normalization methods resulted in a more dispersed calibration but gave consistent results with regard to the identification of bassanite.

However, the normalization does not correct for the difference between the laboratory setup and the flight instrument in the spectrometric instrument response ratio between the UV spectrometer at 248 nm and the VNIR spectrometer at 657 nm. Therefore, a dedicated method was used to determine this specific relative instrument response. Using calibration targets both in the lab and on Mars at similar laser irradiance, we were able to pick spectra that represent plasmas showing similar characteristics, both in the laboratory and on Mars. This is done using graphite and titanium-plate targets on Mars that display C and Ti peaks, respectively, in the two spectral areas of interest. The ratios obtained represent the relative instrument response needed to compare carbon-normalized (C I 248 nm) hydrogen data between the lab and Mars. After proper dark removal, peak fitting, instrument response correction, and normalization to the C peak area at 247.9 nm, the hydrogen data can then be used for comparisons between the laboratory and Mars.

3. Experimental results and application to Gale crater observations

3.1. Calibration curve

The signal obtained in the spectral region of interest, averaged over the 8 analyzed points, is shown in Fig. 1. In the case of the anhydrite pellet, the sample still produces a residual H signal interpreted as due to water molecules tightly bound to the surface, which seem to remain even after heating at 750 °C and is commonly seen in LIBS analyses of hydrogen (Kurniawan et al., 2014). The calibration curve is shown in Fig. 2, with two separate tests performed for each pure calcium sulfate pellet. Normalized H signals from pellet mixtures with gypsum and basalt are also shown along the calibration curve to highlight the linearity of the trend with mixtures. The error bars represent the standard deviation from the spectra of the 8 locations analyzed for each pellet.

3.2. Description of the observations

In Gale crater, calcium sulfate has been detected and analyzed extensively by the ChemCam instrument on 29 different targets observed up to sol (martian day) 360 since Curiosity landing (Nachon et al., 2014). The alpha particle X-ray spectrometer (APXS) instrument also provided elemental composition for a few of the widest calcium sulfate veins. The APXS instrument measured the

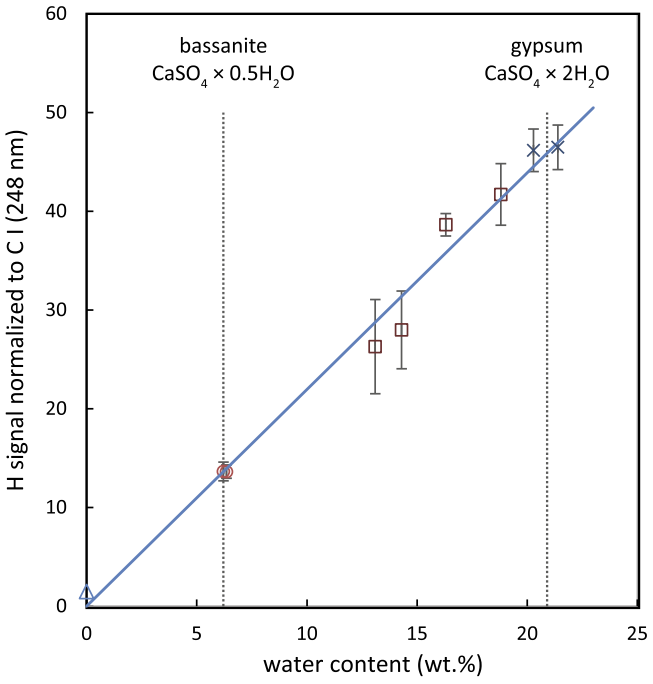

Fig. 2. Hydrogen peak area normalized to carbon peak area at 248 nm as a function of water content of the pellets measured by thermogravimetric analysis. Data points include pellets of anhydrite (triangle), bassanite (circles), gypsum (crosses) and mixtures of gypsum and basalt (squares). The calibration curve is a linear fit with zero intercept (line). The error bars represent the standard deviation from the 8 spectra analyzed for each pellet.

abundance of sulfur but it is not sensitive to hydrogen. APXS has an analytical footprint of 1.7 cm, which was wider than the Ca sulfate features in all cases, with the result that APXS never reported a pure Ca sulfate composition (McLennan et al., 2014) but supported the detection of sulfur and calcium when veins were present within the footprint.

All the ChemCam data obtained up to sol 1248 were classified using imagery and separately using elemental composition results. Based on remote micro-imager (RMI) documentation, points targeting clear white vein material were isolated from other points that were ambiguously mixed with soils or on the edge or outside of a white feature. Sixty-nine different points sampled apparently nearly-pure vein materials (Table S1). Using chemical criteria similar to Nachon et al. (2014), these points were all associated with a detection of sulfur and a high content of calcium. Major-element abundances are provided by calibrated Partial Least Square (Wiens et al., 2013) and Independent Component Analysis (Forni et al., 2013) combined methods for quantification. This re-calibration was completed in 2015 (Clegg et al., submitted). The sulfur signature is detected with ChemCam in the spectra of the calcium sulfate veins but it is not yet fully quantified.

In addition to these exposed vein observations, the rover drill was used several times to collect samples. The drill holes revealed subsurface materials, including small white veins, particularly at two different locations: in a mudstone called John Klein (JK) in the Yellowknife Bay fluvio-lacustrine sediments, and in a sandstone called Telegraph Peak (TP) in the Pahrump Hills at the base of Mount Sharp. These drilling activities enabled us to compare the ChemCam results obtained remotely on the drill hole walls with the results of the XRD and Evolved Gas Analysis (EGA) sample analyses performed by the CheMin and SAM instruments. In John Klein, the vertical ChemCam raster on the drill hole wall hit a white veinlet on the 7th of ten points, where sulfur is detected as well as higher calcium. In Telegraph Peak, a grid of 4 by 4 very closely spaced points was designed to analyze a white vein-

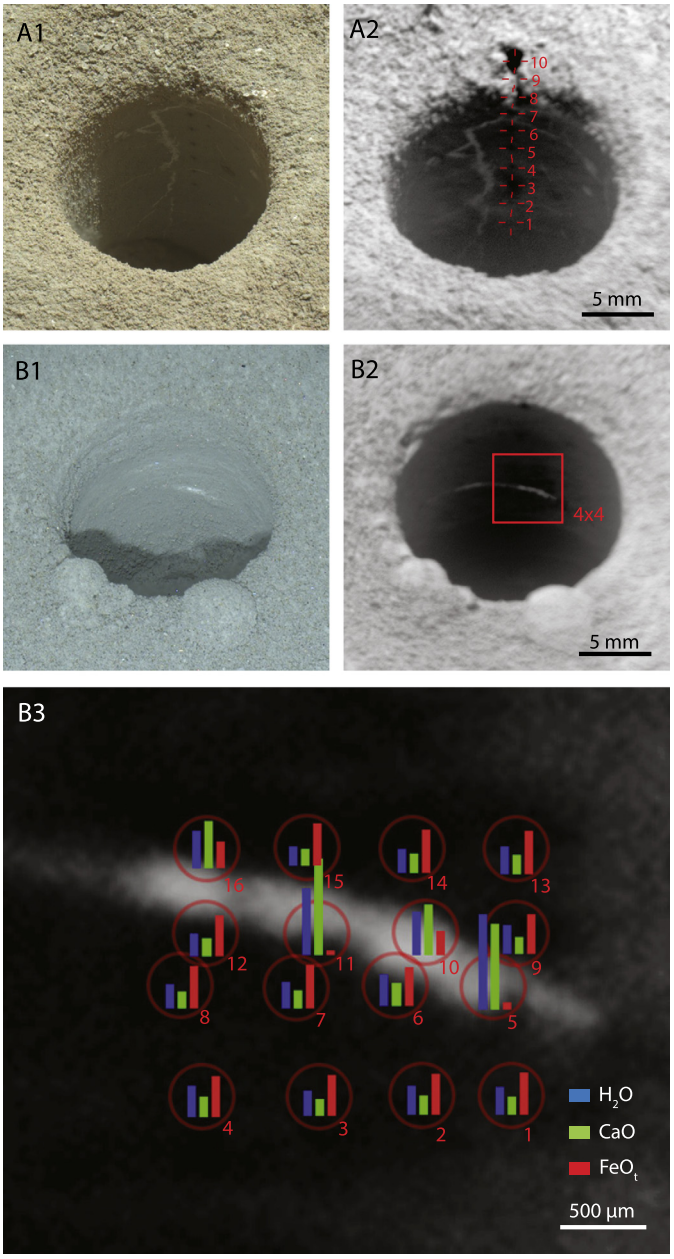

Fig. 3. Imagery from the drill hole analyses: (A1) John Klein (0270MH0252000006R0_DXXX), (A2) RMI image with annotated LIBS spots (CRM_417641715_CCAM01227), (B1) Night-time MAHLI image of the Telegraph Peak drill hole (0911MH0004750000303057R00_DXXX), (B2) RMI image of Telegraph Peak with the approximate location of the 4 × 4 grid of LIBS analyses (CRM_479251063_CCAM03921) (red rectangle) and (B3) close-up of the area analyzed by ChemCam with bar plots (arbitrary scale) showing the variability in water, CaO and FeOT contents.

let seen in the hole. Several points sampled the white material, in some cases mixed with the country rock. Indeed the calcium increased and the iron signal weakened according to the proximity of the points to the white material. Fig. 3 shows the settings for these drill hole observations. The H signal is seen to be strongly correlated with the veinlet material and with the calcium signal, providing strong evidence that it is associated with a hydrated calcium sulfate phase.

3.3. Estimation of vein water content: bassanite detection

After processing and calibration of the data from the previously described observations, the inferred H_2O content is plotted as a

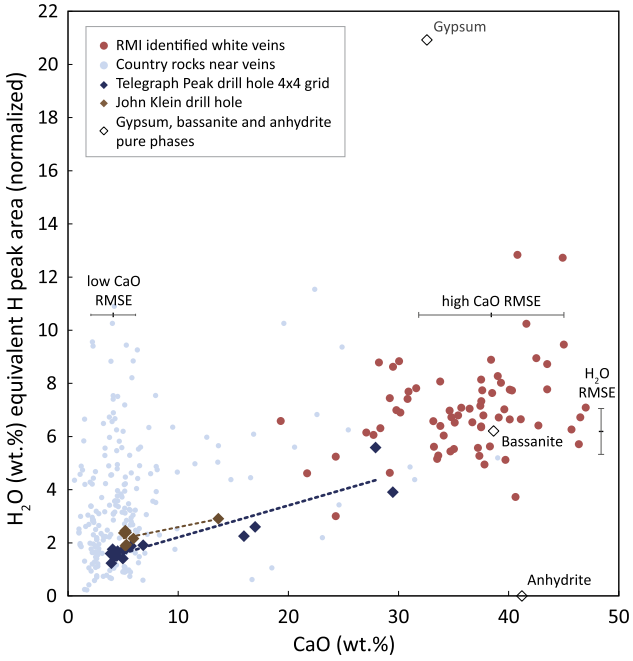

Fig. 4. Water content as a function of CaO content for selected targets at Gale crater. Data include points on white veins identified from RMI images (red circles), points acquired on the country rocks of the same target near and on the edges of the veins (pale blue circles), and points in drill holes (blue and brown diamonds). Positions of pure gypsum, bassanite and anhydrite are shown with black diamonds. Horizontal and vertical errors represent respectively the root mean square error (RMSE) of the estimated CaO and H_2O content. Linear fits of the drill hole data (dashed lines), shown in Fig. 3, trend towards bassanite composition.

function of CaO content in Fig. 4. The 69 points obtained on all the clean and exposed veins cluster around a mean of 6.9 wt.% water content. This value corresponds to the hydration level of bassanite with a theoretical stoichiometric water content at 6.2 wt.%. None of the analysis points plot near gypsum at 20.9 wt.% H_2O, nor close to anhydrite. The root mean square error (RMSE) is 6.5 for such high values of CaO content (Clegg et al., submitted) and a H_2O content RMSE of 1.1 was evaluated using the calibration data in Fig. 2. Dispersion of the CaO and H_2O content is visible in the figure as well. As shown by the data from the country rock and points partially sampling the vein and from drill holes, several points fill the mixing trend with other phases which are mostly less hydrated (Fig. 4). The vertical dispersion seen in the data of nearly pure calcium sulfates, if not solely related to repeatability, could reflect mixtures with small amounts of anhydrite or variations in the bassanite water content. The assumption of 0.5 water of hydration in bassanite depends on relative humidity. Robertson and Bish (2013) have shown that exchange with the atmosphere could possibly occur in the current near-equatorial martian diurnal cycle of water vapor, leading to variable presence of 0.5 to 0.67 H_2O molecules per chemical formula, resulting in water contents varying from 6.2 to 8.1 wt.% in the bassanite. Dedicated tests using ChemCam and REMS will help investigate if such exchange is occurring with the veins at Gale.

The data obtained in the drill holes is shown in Fig. 4 as well. In the Telegraph Peak drill hole, 10 of the 16 points sampled the country rock around the white vein, and their average water content is found to be 1.5 wt.%, which is consistent with the bulk water content provided by EGA of 1.2 wt.%. The 6 remaining points trend along a mixing line toward the bassanite composition with 2 points near 30 wt.% CaO. This trend confirms that the white vein hydration is consistent with bassanite. It is noteworthy that CheMin XRD analysis detected a small amount of calcium sulfate crystalline phases including bassanite and anhydrite in Telegraph

Peak at levels near the detection limit (i.e. <1 wt.%), but no gypsum. This supports the inference that the hydrogen signal seen by ChemCam is characteristic of bassanite, not of gypsum.

At John Klein, the only point with sulfur detection also trends towards bassanite but to a lower extent since most of the points did not sample the vein material. Here as well, CheMin XRD data has shown that bassanite (1.0 wt.%) and anhydrite (2.6 wt.%) were present, but not gypsum (Vaniman et al., 2014). For the 6 first points sampling the country rock in the hole, the average H_2O content is found to be 2.2 wt.%, consistent again with the bulk water content of 2.3 wt.% measured by EGA.

Alternative sources of the hydrogen signal in ChemCam spectra of these veins can also be ruled out. First, although faint peaks of Fe and Mg in the spectra reveal the presence of another material or impurities mixed in the veins, the abundance is very small, as shown by CaO content close to the typical contents of pure calcium sulfate phases. Even if hydrated, such small quantities (a few wt.% at most) cannot contain H_2O in such amounts as to bring the bulk water content near 6.9 wt.%. Second, surface adsorption of water could artificially increase the H signal. However, the measurements were taken during daytime, when relative humidities are very low on Mars (below REMS RH sensitivity of 2%). Moreover, other points within the drill holes would have likely been affected by surface adsorption as well. But Fig. 3 shows that the increase of the H signal is really associated with the vein in Telegraph Peak, and is not seen in the country rock. Finally, the good agreement with the theoretical value of 6.2 wt.% for bassanite, and with SAM analyses for the bulk samples, makes such a hypothesis very unlikely.

To summarize, all the exposed veins analyzed by ChemCam up to sol 1248 are found to consist predominantly of bassanite, and the XRD analyses from CheMin are consistent with the presence of bassanite in the bulk of the samples including veins analyzed by both CheMin and ChemCam instruments. However, anhydrite is found in a roughly similar amount as bassanite by CheMin in the John Klein sample. It should have been sampled at least a few times by ChemCam if it were contained in such amounts in most veins. The absence of pure anhydrite in any of the 69 ChemCam points, the vertical dispersion seen in Fig. 4 and the detection of the two different phases by CheMin XRD analyses, suggests that anhydrite could be a microcrystalline phase mixed within the rock matrix rather than present in the veins, although a small proportion of anhydrite intimately mixed with bassanite in the veins cannot be excluded.

4. Discussion on thermodynamic stability and phase transitions kinetics

Bassanite, or calcium sulfate hemihydrate, is rare on Earth and often a product of alteration, but less frequently it can also be a primary mineral. It is found associated with gypsum in most cases. Bassanite was identified in volcanic ejecta (Spencer, 1913) and interpreted as dehydrated gypsum, but not as a magmatic mineral. It is also reported in directly deposited fumarolic mineral assemblages (Balić-Žunić et al., 2009). The largest occurrences of bassanite are found in highly arid zones and interpreted to be a dehydration product of gypsum at or near the surface: bassanite was found in salt lake deposits at shallow depths associated with gypsum gradually dehydrated from top to down (Mees, 1998) and in fluvial sediments that underwent hydration/dehydration cycles (Mees and De Dapper, 2005). Bassanite was also found in association with gypsum in a desert lake basin at burial depths greater than about 150 m (Allen and Kramer, 1953). Thin bassanite coatings around sand grains have formed by topotactic replacement of gypsum in an arid desert environment, in the absence of liquid water (Mees and Stoops, 2003). Bassanite was also reported in a semi-arid environment, in shallow acidic and saline desiccated soils (Benison and Bowen, 2013), as well as in the upper section of gypsum-rich soil profiles (Akpokodje, 1984). In the latter case the bassanite/gypsum transition occurs at the depth of moisture penetration from below.

To our knowledge there is no site on Earth like Gale crater with a setting of millimeters to centimeters thick bassanite veins cross-cutting sedimentary country rocks. As a secondary mineral, bassanite most probably comes from the dehydration of gypsum. We do not consider bassanite hydration directly from anhydrite because there is no evidence in the literature for intermediate bassanite in the hydration process of anhydrite to gypsum (Hardie, 1967; Billo, 1987; Freyer and Voigt, 2003). On Earth, anhydrite is found in large amounts exposed at the surface in the saline and dry environments of sabkhas and is only seen to hydrate in the presence of liquid water (Warren, 1991). Under current conditions at Gale crater where the average humidity is much lower than in terrestrial deserts, and where liquid water or ice are not stable at the surface, the hydration of anhydrite is very unlikely. The Rocknest aeolian sand shadow analyzed by Curiosity at Gale crater was exposed at the surface for a substantially long period of time and yet anhydrite, and not bassanite or gypsum, was observed there (Bish et al., 2013). This confirms the inability of anhydrite to hydrate when exposed extensively to the current climate. Furthermore, high pressures are not considered in the following discussion on bassanite formation for the following reasons: bassanite was suggested to be stable in the presence of aqueous solution for a specific temperature range and only at pressures higher than 235 MPa (Yamamoto and Kennedy, 1969; Mirwald, 2006); if Gale crater was once completely filled, burying the calcium sulfates under 5 km of 2000 $kg\,m^{-3}$ sediments, the pressure achieved would not have exceeded ~40 MPa. Therefore, even if the aqueous event occurred at maximum burial, bassanite cannot be explained here by the high pressure effect, and temperature, water activity, or kinetic effects, should be invoked instead.

When calcium sulfates precipitate from solution, it has been shown that bassanite is a nano-phase precursor to the formation of gypsum (Van Driessche et al., 2012), but it is also a precursor of anhydrite in solution for potentially year-long durations (Ossorio et al., 2014), suggesting that bassanite could also have formed from direct precipitation under specific conditions.

For all the reasons mentioned previously, the discussion will focus on two scenarios, 1) direct precipitation of bassanite in aqueous solution, and 2) formation of gypsum veins first, then dehydration to bassanite due to desiccation in arid conditions. Fig. 5 summarizes thermodynamic equilibria of calcium sulfate phases overlaid with kinetic behavior results as a function of water activity and temperature. Boxes are used to represent the range of temperature and water activity of specific experiments reported here. Fig. 5(A) shows the thermodynamic equilibrium between anhydrite and gypsum in aqueous solution with variable water activity. Kinetic results from Ossorio et al. (2014) highlight the time-limited presence in solution of bassanite and gypsum in the anhydrite stability field. Fig. 5(B) shows experimental results for calcium sulfate phase transitions in air, where water activity corresponds to relative humidity. Bassanite dehydration to insoluble anhydrite is not represented here in this case but was reported to occur between 200 and 600 °C (Freyer and Voigt, 2003). The bassanite to soluble anhydrite reversible transition and gypsum to bassanite irreversible dehydration boundary from Oetzel et al. (2000) are shown. Additionally, extrapolated kinetic results on the dehydration of gypsum to bassanite from Robertson and Bish (2013) are represented as well, using dotted lines. These extrapolated kinetic trends should be considered indicative. In particular, the behavior at low temperatures is unknown.

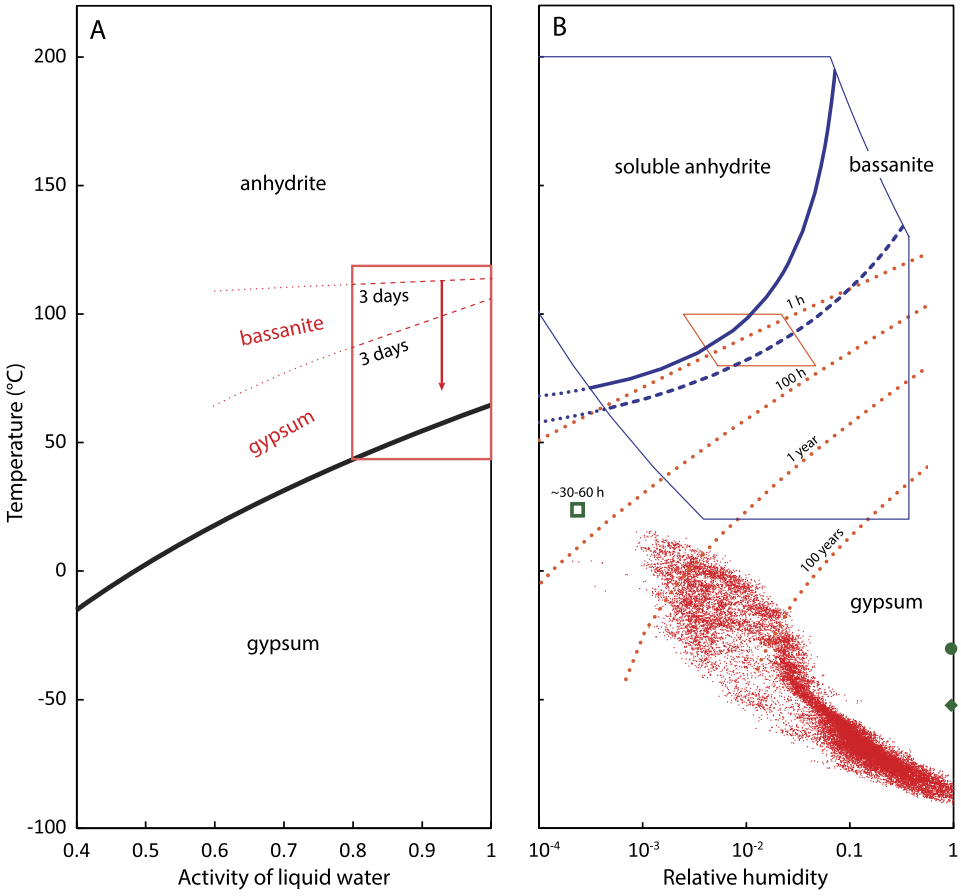

Fig. 5. Calcium sulfate stability and kinetic data as a function of temperature and water activity, for an aqueous solution (A), and for different relative humidities (B). (A) Gypsum/anhydrite transition in aqueous solution (black line) (Raju and Atkinson, 1990; Freyer and Voigt, 2003) and the range covered by the kinetics experiments of Ossorio et al. (2014) (red lines and arrow). Kinetic boundaries (i.e. boundaries delimiting the phases found in solution after a specific timing) of the latter study are reported (red dashed lines) and represent the precursor phases found in solution after 3 days, with subsequent evolution path leading to the formation of anhydrite (red arrow). Extrapolated trends to lower water activities are shown in dotted red lines, and are only indicative. (B) Robertson and Bish (2013) investigated the time needed to start dehydration of gypsum (orange dotted lines) based on experiments performed in a specific narrow range (orange box). Dehydration of gypsum to bassanite at 0.7 Pa vapor pressure and 24 °C took ~30–60 h to initiate (green square) (Vaniman and Chipera, 2006). Additionally, bassanite hydration experiments in the presence of ice were performed for long durations (Vaniman et al., 2009): at −30 °C bassanite fully hydrated to gypsum in 2 yrs (green circle), but no gypsum was observed at −53 °C after 3 yrs (green diamond). Experiments by Oetzel et al. (2000) performed in a large range of temperature and air moisture (water vapor pressures range between 0.1 and 1000 mbar) (blue polygon) indicate reversible soluble anhydrite/bassanite transition (blue line), and irreversible gypsum to bassanite dehydration (dashed blue line). The duration of their experiment was not reported. Extrapolation of the transition trends to low RH are also represented (dotted blue lines). Hourly surface relative humidities and temperatures at Gale crater as derived from REMS data are shown in red. It represents the extent of diurnal variations over more than a Martian year, under which bassanite has been identified (this study).

4.1. Direct precipitation of bassanite

Bassanite is a precursor to anhydrite precipitation for specific temperatures and water activity ranges: Ossorio et al. (2014) have shown that anhydrite growth rate is strongly dependent on temperature and is preceded by rapidly-formed bassanite. This is also true near the gypsum-anhydrite equilibrium, where bassanite forms massively first, followed by anhydrite formation only after some time in solution. Gypsum can even form at temperatures above its equilibrium, but will ultimately turn into anhydrite if still in contact with solution at these temperatures. Moreover, temperatures must remain relatively high for bassanite to persist for some time under aqueous conditions and not turn readily into gypsum (Fig. 5(A)). The effect of decreasing water activity is to increase the persistence time of the bassanite precursor: in a saline solution (water activity ~0.8) bassanite precipitates first for up to 2 months at 80 °C before turning into anhydrite (Ossorio et al., 2014). It has been suggested that the salinity of waters on Mars may have reached extreme levels (water activity down to 0.5) in a number of localities (Tosca et al., 2008). To our knowledge the phase transition kinetics of calcium sulfates was not tested down to such extremely low water activities, but we can expect it would have resulted in the preservation of bassanite for even longer times in solution. These findings are particularly relevant to evaporitic environments where salinity reduces water activity. It was also reported that ions like phosphates act as retarders in the crystallization of gypsum and stabilize bassanite in solution (Wang and Meldrum, 2012). For example, this effect is suspected to stabilize bassanite found in crusts on the walls of caves containing large phosphate deposits (Onac and Veres, 2003), but at Gale crater no evidence for such impurities could be found within veins. In addition, there is yet no evidence of low water activities related to the presence of high-solubility salts (e.g. chlorides) in the veins, which would be found in such concentrated brines.

Direct precipitation of millimeter to centimeter thick bassanite veins – as seen at Gale crater – remains unlikely because of the narrow range of high temperatures and durations needed to avoid producing anhydrite or gypsum instead. Yet no evidence for bulk anhydrite has been found in the veins analyzed so far at Gale. This sets an upper limit, discussed below, for the precipitation temperature of the veins.

4.2. Bassanite from gypsum dehydration

In this scenario, gypsum precipitated in the veins and then dehydrated into bassanite. Freyer and Voigt (2003) summarize the results of calcium sulfate thermodynamic stability in solution as a function of temperature and water activity. For gypsum to precipitate from solution, temperatures should be lower than 60 °C for a water activity of 1, and 27 °C for 0.7, otherwise bulk anhydrite would ultimately form (Fig. 5(A)). Therefore, from thermodynamic constraints, temperature had to remain below 60 °C when gypsum precipitated from the fluids at Gale crater. Subsequently, gypsum could have dehydrated into bassanite following exposure to hyperarid conditions. Indeed, bassanite has been documented on Earth mostly in arid settings (see references above), and it is known as plaster of Paris when produced from gypsum dehydration by heating in air. This dehydration process has been studied under various relative humidities (Fig. 5B) (Oetzel et al., 2000). A notable difference on Mars is the much lower surface temperature, which would imply much slower rates. There have been no long-exposure experiments of gypsum dehydration under truly martian conditions but a few experiments at higher temperatures and extrapolated to Mars suggest that dehydration could occur, but on a much longer time-scale than current diurnal and seasonal cycles (Fig. 5(B)) (Vaniman and Chipera, 2006; Robertson and Bish, 2013). Orbital data further suggests that bassanite is found in other sites at low latitudes (Mangold et al., 2010; Wray et al., 2010), and could therefore be more prevalent than gypsum under these climatic conditions. This dehydration process would be more efficient at depth due to higher subsurface temperatures, as a result of the geothermal gradient. Alternatively, dehydration could have been induced by impact-generated heat (Robertson and Bish, 2013). Although ChemCam observations done so far are mostly consistent with bassanite, the slow dehydration kinetics, not well constrained, do not rule out the possibility of minor gypsum residues in the sediments.

Once bassanite is formed, hydration to gypsum is unlikely at Gale crater. Vaniman et al. (2009) tested hydration of bassanite in contact with ice at low temperatures for as long as 3 yrs and found very sluggish gypsum formation, and at −53 °C, no gypsum was formed in this time interval. In Gale crater, frost was not directly identified, and environmental data from REMS (Fig. 5(B)) suggests that conditions for frost formation have been met only for a few nights in the first martian year that Curiosity spent on Mars, possibly resulting in the condensation of only a few tenths of microns of water ice (Martínez et al., 2015).

Although our observations are consistent with the presence of gypsum during the last contact with liquid water in the veins and subsequent dehydration to bassanite under more arid conditions, they do not rule out former distinct aqueous events. For instance, anhydrite could have been formerly present in the veins due to low water activity or high temperatures due to burial. It could then have hydrated to gypsum due to the presence of low temperature fluids as documented on Earth in a number of cases (Warren, 2006). In such cases, anhydrite hydration to gypsum is known to cause hydrofracturing of the bedrock (Shearman et al., 1972; Cosgrove, 2001; Philipp, 2008), which may explain the presence of a network of millimeter size veinlets along with thicker veins as seen by Curiosity (Nachon et al., 2014).

To date, no thick veins have been analyzed by CheMin so the vein mineralogy has not yet been examined by X-ray diffraction. The prevalence of anhydrite in CheMin XRD analyses of bulk sample still needs to be explained. Our results suggest the most likely hypothesis is that anhydrite is present in the bedrock, but absent or less common in veins. If anhydrite formed at an earlier stage within the sediments, it could suggest that the compaction was such that rock porosity remained below the percolation threshold, isolating the anhydrite from water within the fractures where gypsum precipitated. Alternatively, the fluids could have percolated through the sediments and anhydrite could have formed locally due to higher salinity within the bedrock.

5. Conclusions

On Mars, in-situ analyses of water have been scarce and limited to analyses of bulk samples by pyrolysis. ChemCam has the ability to detect hydrogen far more frequently and at a much finer spatial scale, typical of many diagenetic features observed by Curiosity. For instance, this enables a better assessment of the hydration states of salts and alteration products. The experiments reported here focused on the calibration of the hydrogen signal with a series of calcium sulfate samples, which complements rare laboratory data found in the literature on the quantification of hydrogen by the LIBS technique. Using a calibration of the hydrogen signal measured by ChemCam, our study indicates that the white veins crosscutting sediments found in Gale crater are made predominantly of bassanite.

Because anhydrite is not found to hydrate under current conditions on Mars and the time and temperature range for bassanite direct precipitation is narrow, gypsum likely formed (either directly or as a result of anhydrite hydration under low-T, low-salinity aqueous conditions) and then dehydrated to bassanite. Gypsum formation implies that during the last presence of water in the veins, the temperature did not exceed 60 °C, otherwise anhydrite would have been found instead. Given current possible hypotheses on geothermal gradients and paleoclimates used by Borlina et al. (2015), this temperature limit could represent a maximum burial depth of 1.5 to 3 km during the Hesperian climate if the fluid temperature followed geothermal profiles. The subsequent formation and persistence of bassanite from gypsum found in the veins is consistent with hyperarid conditions and favored by burial or impacts, which would have increased the temperature of the sediments. The occurrence of anhydrite found in a mudstone crosscut by the veins remains to be explained. It could have formed separately, perhaps at higher temperature or due to the presence of more saline water percolating through the bedrock, before the formation of gypsum that ultimately dehydrated to produce bassanite.

Acknowledgements

This research was funded by Université Paul Sabatier as part of a PhD thesis, and experiments were conducted at Institut de Recherche en Astrophysique et Planétologie (IRAP) with support from CNES. Funding for MSL and ChemCam operations and science in the US were provided by the NASA Mars Exploration Program. Funding for ChemCam operations in France was provided by CNES. The authors gratefully acknowledge the support of all of the people at JPL involved in making MSL a successful mission. The Raman spectroscopy analysis to assess the purity of the calcium sulfate pellets was performed by Olivier Beyssac and Sylvain Bernard from the Institut de Minéralogie, de Physique des Matériaux et de Cosmochimie (IMPMC). The authors thankfully recognize their valuable help. The authors also thank Mikhail Zolotov and one anonymous reviewer for their helpful comments.

Appendix A. Supplementary material

Supplementary material related to this article can be found online at http://dx.doi.org/10.1016/j.epsl.2016.07.045.

References

Akpokodje, E.G., 1984. The occurrence of bassanite in some Australian arid-zone soils. Chem. Geol. 47 (3–4), 361–364. http://dx.doi.org/10.1016/0009-2541(84)90135-9.

Allen, R.D., Kramer, H., 1953. Occurence of bassanite in two desert basins in southeastern California. U.S. Geol. Surv. 38, 1266–1268.

Audouard, J., Poulet, F., Vincendon, M., Bibring, J.-P., Forget, F., Langevin, Y., Gondet, B., 2014. Mars surface thermal inertia and heterogeneities from OMEGA/MEX. Icarus 233, 194–213. http://dx.doi.org/10.1016/j.icarus.2014.01.045.

Balić-Žunić, T., Garavelli, A., Acquafredda, P., Leonardsen, E., Jakobsson, S.P., 2009. Eldfellite, $NaFe(SO_4)_2$, a new fumarolic mineral from Eldfell volcano, Iceland. Mineral. Mag. 73 (1), 51–57. http://dx.doi.org/10.1180/minmag.2009.073.1.51.

Benison, K.C., Bowen, B.B., 2013. Extreme sulfur-cycling in acid brine lake environments of Western Australia. Chem. Geol. 351, 154–167. http://dx.doi.org/10.1016/j.chemgeo.2013.05.018.

Billo, S.M., 1987. Petrology and kinetics of gypsum–anhydrite transitions. J. Pet. Geol. 10 (1), 73–85. http://dx.doi.org/10.1111/j.1747-5457.1987.tb00997.x.

Bish, D.L., et al., 2013. X-ray diffraction results from mars science laboratory: mineralogy of rocknest at gale crater. Science 341 (6153), 1238932. http://dx.doi.org/10.1126/science.1238932.

Bishop, J.L., Lane, M.D., Dyar, M.D., King, S.J., Brown, A.J., Swayze, G.A., 2014. Spectral properties of Ca-sulfates; gypsum, bassanite, and anhydrite. Am. Mineral. 99 (10), 2105–2115. http://dx.doi.org/10.2138/am-2014-4756.

Borlina, C.S., Ehlmann, B.L., Kite, E.S., 2015. Modeling the thermal and physical evolution of Mount Sharp's sedimentary rocks, Gale Crater, Mars: implications for diagenesis on the MSL Curiosity rover traverse. J. Geophys. Res., Planets 120 (8), 2015JE004799. http://dx.doi.org/10.1002/2015JE004799.

Clegg et al., submitted. Recalibration of the Mars Science Laboratory ChemCam Instrument with an Expanded Geochemical Database, Spectrochim. Acta B.

Cosgrove, J.W., 2001. Hydraulic fracturing during the formation and deformation of a basin; a factor in the dewatering of low-permeability sediments. AAPG Bull. 85 (4), 737–748. http://dx.doi.org/10.1306/8626C997-173B-11D7-8645000102C1865D.

Forni, O., Maurice, S., Gasnault, O., Wiens, R.C., Cousin, A., Clegg, S.M., Sirven, J.-B., Lasue, J., 2013. Independent component analysis classification of laser induced breakdown spectroscopy spectra. Spectrochim. Acta, Part B, At. Spectrosc. 86, 31–41. http://dx.doi.org/10.1016/j.sab.2013.05.003.

Freyer, D., Voigt, W., 2003. Crystallization and Phase Stability of $CaSO_4$ and $CaSO_4$ – based salts. Monatsh. Chem. 134 (5), 693–719. http://dx.doi.org/10.1007/s00706-003-0590-3.

Gendrin, A., et al., 2005. Sulfates in Martian layered terrains: the OMEGA/Mars express view. Science 307 (5715), 1587–1591. http://dx.doi.org/10.1126/science.1109087.

Gilmore, M.S., Greenwood, J.P., 2009. Gypsum and associated sulfates in Iani Chaos, Mars. AGU Fall Meet. 21, 4.

Hardie, L.A., 1967. The gypsum–anhydrite equilibrium at one atmosphere pressure. Am. Mineral. 52, 171–200.

Kurniawan, K.H., Tjia, M.O., Kagawa, K., 2014. Review of laser-induced plasma, its mechanism, and application to quantitative analysis of hydrogen and deuterium. Appl. Spectrosc. Rev. 49 (5), 323–434. http://dx.doi.org/10.1080/05704928.2013.825267.

Langevin, Y., Poulet, F., Bibring, J.-P., Schmitt, B., Douté, S., Gondet, B., 2005. Summer evolution of the north polar cap of Mars as observed by OMEGA/Mars express. Science 307 (5715), 1581–1584. http://dx.doi.org/10.1126/science.1109438.

Le Mouélic, S., et al., 2015. The ChemCam remote micro-imager at gale crater: review of the first year of operations on Mars. Icarus 249, 93–107. http://dx.doi.org/10.1016/j.icarus.2014.05.030.

Mangold, N., Roach, L., Milliken, R., Le Mouélic, S., Ansan, V., Bibring, J.P., Masson, P., Mustard, J.F., Murchie, S., Neukum, G., 2010. A late Amazonian alteration layer related to local volcanism on Mars. Icarus 207, 265–276. http://dx.doi.org/10.1016/j.icarus.2009.10.015.

Martínez, G.M., et al., 2015. Potential sub-micrometer-thick frost events and soil water content at gale crater: calculations from MSL/REMS measurements, vol. 46, p. 2277.

Maurice, S., et al., 2012. The ChemCam instrument suite on the mars science laboratory (MSL) rover: science objectives and mast unit description. Space Sci. Rev. 170 (1–4), 95–166. http://dx.doi.org/10.1007/s11214-012-9912-2.

McLennan, S.M., et al., 2014. Elemental geochemistry of sedimentary rocks at Yellowknife Bay, Gale Crater, Mars. Science 343 (6169), 1244734. http://dx.doi.org/10.1126/science.1244734.

Mees, F., 1998. The alteration of glauberite in lacustrine deposits of the Taoudenni–Agorgott basin, northern Mali. Sediment. Geol. 117 (3–4), 193–205. http://dx.doi.org/10.1016/s0037-0738(98)00042-6.

Mees, F., De Dapper, M., 2005. Vertical variations in bassanite distribution patterns in near-surface sediments, southern Egypt. Sediment. Geol. 181 (3–4), 225–229. http://dx.doi.org/10.1016/j.sedgeo.2005.09.002.

Mees, F., Stoops, G., 2003. Circumgranular bassanite in a gypsum crust from eastern Algeria – a potential palaeosurface indicator. Sedimentology 50 (6), 1139–1145. http://dx.doi.org/10.1046/j.1365-3091.2003.00598.x.

Meslin, P.-Y., et al., 2013. Soil diversity and hydration as observed by ChemCam at gale crater, Mars. Science 341 (6153), 1238670. http://dx.doi.org/10.1126/science.1238670.

Mirwald, P.W., 2006. Dehydration study of gypsum–bassanite–anhydrite up to 3.5 GPa-indication of PVT anomalies of water at high pressure. Geophys. Res. Abstr. 8, 2724.

Nachon, M., et al., 2014. Calcium sulfate veins characterized by ChemCam/Curiosity at Gale crater, Mars. J. Geophys. Res., Planets 119 (9), 2013JE004588. http://dx.doi.org/10.1002/2013JE004588.

Oetzel, M., Heger, G., Koslowski, T., 2000. Einfluss von Umgebungsfeuchte und Temperatur auf die Phasenumwandlungen im System $CaSO_4$–H_2O. ResearchGate 53, 254–361.

Onac, B.P., Veres, D.S., 2003. Sequence of secondary phosphates deposition in a karst environment: evidence from Magurici Cave (Romania). Eur. J. Mineral. 15 (4), 741–745. http://dx.doi.org/10.1127/0935-1221/2003/0015-0741.

Ossorio, M., Van Driessche, A.E.S., Pérez, P., García-Ruiz, J.M., 2014. The gypsum–anhydrite paradox revisited. Chem. Geol. 386, 16–21. http://dx.doi.org/10.1016/j.chemgeo.2014.07.026.

Philipp, S.L., 2008. Geometry and formation of gypsum veins in mudstones at Watchet, Somerset, SW England. Geol. Mag. 145 (6), 831–844. http://dx.doi.org/10.1017/S0016756808005451.

Raju, K.U.G., Atkinson, G., 1990. The thermodynamics of "scale" mineral solubilities. 3. Calcium sulfate in aqueous sodium chloride. J. Chem. Eng. Data 35 (3), 361–367. http://dx.doi.org/10.1021/je00061a038.

Rice, M.S., et al., 2013. Hydrated minerals at yellowknife bay, gale crater, Mars: observations from Mastcam's science filters, vol. 23, p. 1795.

Robertson, K., Bish, D., 2013. Constraints on the distribution of $CaSO_4 \cdot nH_2O$ phases on Mars and implications for their contribution to the hydrological cycle. Icarus 223 (1), 407–417. http://dx.doi.org/10.1016/j.icarus.2012.10.028.

Schröder, S., et al., 2015. Hydrogen detection with ChemCam at Gale crater. Icarus 249, 43–61. http://dx.doi.org/10.1016/j.icarus.2014.08.029.

Shearman, D.J., Mossop, G., Dunsmore, H., Martin, M., 1972. Origin of gypsum veins by hydraulic fracture. J. Inst. Min. Metall. B 149–155.

Spencer, L.J., 1913. Sixth list of new mineral names. Bassanite. Mineral. Mag. 16 (354).

Squyres, S.W., 2012. Clues to a hot, wet and violent ancient Mars: spirit in the Columbia hills and opportunity at Endeavour Crater. AGU Fall Meet. Abstr. 33, 3.

Tosca, N.J., Knoll, A.H., McLennan, S.M., 2008. Water activity and the challenge for life on early Mars. Science 320 (5880), 1204–1207. http://dx.doi.org/10.1126/science.1155432.

Van Driessche, A.E.S., Benning, L.G., Rodriguez-Blanco, J.D., Ossorio, M., Bots, P., García-Ruiz, J.M., 2012. The role and implications of bassanite as a stable precursor phase to gypsum precipitation. Science 336 (6077), 69–72. http://dx.doi.org/10.1126/science.1215648.

Vaniman, D.T., Chipera, S.J., 2006. Transformations of Mg- and Ca-sulfate hydrates in Mars regolith. Am. Mineral. 91 (10), 1628–1642. http://dx.doi.org/10.2138/am.2006.2092.

Vaniman, D.T., Bish, D.L., Chipera, S.J., 2009. Bassanite on Mars, vol. 40, p. 1654.

Vaniman, D.T., et al., 2014. Mineralogy of a mudstone at yellowknife bay, Gale Crater, Mars. Science 343 (6169), 1243480. http://dx.doi.org/10.1126/science.1243480.

Wang, Y.W., Meldrum, F.C., 2012. Additives stabilize calcium sulfate hemihydrate (bassanite) in solution. J. Mater. Chem. 22 (41), 22055–22062. http://dx.doi.org/10.1039/c2jm34087a.

Warren, J.K., 1991. Sulfate dominated sea-marginal and platform evaporative settings. Chapter 2. In: Developments in Sedimentology, vol. 50. Elsevier, pp. 69–187.

Warren, J.K., 2006. Evaporites: Sediments, Resources and Hydrocarbons. Springer Science & Business Media.

Weitz, C.M., Bishop, J.L., Grant, J.A., 2013. Gypsum, opal, and fluvial channels within a trough of Noctis Labyrinthus, Mars: implications for aqueous activity during the Late Hesperian to Amazonian. Planet. Space Sci. 87, 130–145. http://dx.doi.org/10.1016/j.pss.2013.08.007.

Wiens, R.C., et al., 2012. The ChemCam instrument suite on the Mars science laboratory (MSL) rover: body unit and combined system tests. Space Sci. Rev. 170 (1–4), 167–227. http://dx.doi.org/10.1007/s11214-012-9902-4.

Wiens, R.C., et al., 2013. Pre-flight calibration and initial data processing for the ChemCam laser-induced breakdown spectroscopy instrument on the Mars Science Laboratory rover. Spectrochim. Acta, Part B, At. Spectrosc. 82, 1–27. http://dx.doi.org/10.1016/j.sab.2013.02.003.

Wray, J.J., Squyres, S.W., Roach, L.H., Bishop, J.L., Mustard, J.F., Noe Dobrea, E.Z., 2010. Identification of the Ca-sulfate bassanite in Mawrth Vallis, Mars. Icarus 209, 416–421. http://dx.doi.org/10.1016/j.icarus.2010.06.001.

Yamamoto, H., Kennedy, G.C., 1969. Stability relations in the system $CaSO_4$–H_2O at high temperatures and pressures. Am. J. Sci. A 267, 550–557.